Ghost stochastic resonance with distributed inputs in pulse-coupled electronic neurons

Abel Lopera,[1] Javier M. Buldú,[1,*] M. C. Torrent,[1] Dante R. Chialvo,[2] and Jordi García-Ojalvo[1,†]
[1]*Departamento de Física i Enginyeria Nuclear, Universitat Politècnica de Catalunya, Colom 11, E-08222 Terrassa, Spain*
[2]*Department of Physiology, Northwestern University, Chicago, Illinois 60611, USA*
(Received 29 September 2005; published 8 February 2006)

We study experimentally the phenomenon of ghost stochastic resonance in pulse-coupled excitable systems, for input signals distributed among different elements. Specifically, two excitable electronic circuits are driven by different sinusoidal signals that produce periodic spikes at distinct frequencies. Their outputs are sent to a third circuit that processes these spiking signals and is additionally perturbed by noise. When the input signals are harmonics of a certain fundamental (that is not present in the inputs) the processing circuit exhibits, for an optimal amount of noise, a resonant response at the frequency of the missing fundamental (ghost frequency). In contrast with the standard case in which the signals being directly integrated are sinusoidal, this behavior relies here on a coincidence-detection mechanism. When the input signals are homogeneously shifted in frequency, the processing circuit responds with pulse packages composed of spikes at a frequency that depends linearly on the frequency shift. Expressions for the dependence of the package period and duration on the frequency shift and spike width, respectively, are obtained. These results provide an experimental verification of a recently proposed mechanism of binaural pitch perception.

DOI: 10.1103/PhysRevE.73.021101 PACS number(s): 05.40.−a, 05.45.−a

I. INTRODUCTION

Stochastic resonance (SR) has become a paradigm of noise-enhanced signal detection in nonlinear systems [1,2]. Most SR studies have concentrated on simple harmonic signals, although some attention has also been paid to signals with complex spectra, such as multifrequency [3], noisy [4], and aperiodic [5] signals. Those studies have been mostly restricted so far to noise-enhanced amplification and detection, but complex signals also need to be *processed*. The term "processing" refers here to the ability to extract a single quantitative feature from a complex signal with a multifeatured spectrum. A classical example is the perception of the pitch of complex sounds, through which our brain is able to extract a quantitative attribute from a multifrequency sound and compare it on a one-dimensional scale with pure harmonic (i.e., single-frequency) sounds.

Recently, a mechanism has been proposed that addresses both signal detection and processing enhanced by noise in excitable systems. Via this mechanism, named ghost stochastic resonance (GSR), an excitable element driven by several sinusoidal inputs, all of them harmonics of (but different from) a certain fundamental frequency, responds optimally to the missing fundamental (ghost frequency) for an intermediate amount of noise [6]. When the signals are rendered inharmonic (by applying a frequency shift equally to all of them), the system responds with a linear shift in the response frequency, which agrees with previous psychophysical experiments if that response frequency is identified with the perceived pitch [7]. GSR has been observed experimentally in semiconductor lasers [8,9] and in electronic circuits [10].

The ghost resonance mechanism described above relies on two basic features: (i) the individual frequencies composing the complex tones add linearly, producing peaks of constructive interference whose amplitude is always insufficient to trigger individually the system's output; and (ii) the system threshold is reached with noise, which naturally selects the maximum constructive interferences. The spacing of these maxima, and consequently the system's pulsed output, occurs at the ghost frequency, whose detection can be optimized by noise following a standard SR mechanism. One can thus say that processing in this case takes place before detection, and is performed through a straightforward linear summation of the input signals. In other situations, however, processing either is interwoven with detection, or takes place after it. This happens, for instance, when the input signals are distributed among different detecting elements. In that case, processing has to occur after detection, and has to be mediated by the coupling between the detecting elements. Such a situation has been experimentally investigated in mutually coupled semiconductor lasers, with two different harmonics being applied to each of two lasers. Successful response at the ghost frequency was reported in that case [11].

The processing of distributed inputs has also physiological functionalities. An example is binaural pitch perception, where input harmonics are separately presented to human subjects through different ears and the missing fundamental is still perceived [12]. The GSR mechanism can be extended to describe this situation by taking into account that the different inputs are transduced by distinct detector neurons into spike trains of different frequencies, and integrated by a third neuron in a deeper processing layer of the auditory system. Such a model has been recently studied by means of numerical simulations, yielding the expected GSR effect [13]. This mechanism can also apply for arrival time detection and comparison between left and right ear, whenever arrival times have to be differentially processed between different receptor organs (for instance, in the processing of interaural

*Electronic address: javier.martin-buldu@upc.edu; URL: http://xuncla.upc.es/javier
†Electronic address: jordi.g.ojalvo@upc.edu

time differences for sound localization in mammals [14]).

In this paper we present an experimental realization of this mechanism, implemented in pulse-coupled nonlinear electronic circuits operating in an excitable regime. The results obtained, besides providing experimental verification of the phenomenon, give us further insight into the structure of the resulting processing signal in the presence of inharmonicity. In what follows, after describing the specifics of the electronic circuits used in our study (Sec. II), we show evidence of the existence of GSR (Sec. III), followed by a description of the inharmonic case (Sec. IV), and an analysis of the response of the processing circuit in that case, which has the form of pulse packages that can be fully characterized (Sec. V).

II. EXPERIMENTAL SYSTEM

Our model system is an excitable version of the so-called Chua circuit [15], shown in Fig. 1(a). This circuit contains a nonlinear resistor connected to a set of passive electronic components. Different dynamical regimes arise for different values of the resistor R_{exc}, including stable, periodic, excitable, and chaotic dynamics. We tune the circuit into an excitable regime by setting $R_{\text{exc}}=270\ \Omega$. This regime is characterized by excursions away from a stable state when an external perturbation exceeds a certain threshold [16]. The external perturbation is provided by an input signal at V_1 [see Fig. 1(a)], applied through a voltage follower combined with a discharge resistance of 2 kΩ [15]. The excursions take the form of voltage pulses in the circuit's output; a typical example is shown in Fig. 1(b). All experimental results obtained in this paper have been reproduced by numerical simulations of the circuit (results not shown).

The experimental setup is schematically depicted in Fig. 2. Two input circuits are harmonically driven at two different frequencies, f_1 and f_2, generated by an Agilent 33250A function generator. The modulation amplitude of both signals is set above the excitable threshold of the circuits, in order to induce periodic spiking at their outputs. The outputs V_1 [see Fig. 1(a)] of both circuits are sent to a third, processing circuit via a voltage follower (which guarantees unidirectional coupling) and an electronic adder. The latter also receives a noisy signal with a bandwidth of 80 MHz, produced by the function generator, and whose intensity can be adjusted.

III. INFLUENCE OF NOISE

The processing circuit is set to operate in the subthreshold regime in the absence of noise. This is possible by adjusting the voltages coming from the two input circuits (via a voltage adder with variable gain) to a subthreshold value, so that the sum of the two input spiking signals is not strong enough to produce spiking in the third circuit without noise (the role of noise in the dynamics is crucial in that sense). The two input frequencies have the form

$$f_1 = kf_0 + \Delta f, \quad f_2 = (k+1)f_0 + \Delta f, \tag{1}$$

where f_0 is the fundamental frequency, $k>1$ is an integer, and Δf is a frequency detuning. In our particular case, we

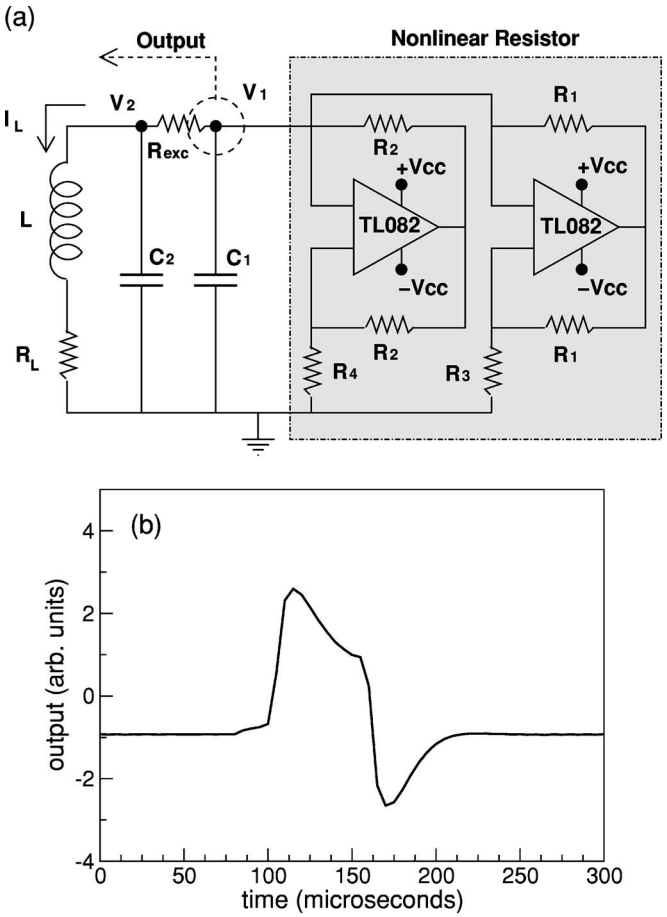

FIG. 1. (a) Scheme of an excitable Chua circuit, which is constructed with two TL082 operational amplifiers and passive electronic components of values: $L=10$ mH, $C_1=10$ nF, $C_2=1$ nF, $V_{cc}=5$ V, $R_1=10$ kΩ, $R_2=270\ \Omega$, $R_3=1$ kΩ, $R_4=220\ \Omega$, $R_L=20\ \Omega$. We set $R_{\text{exc}}=270\ \Omega$ in order to have excitable dynamics. V_1 corresponds to the output of the circuit, which is coupled to a secondary Chua through a voltage follower. (b) Typical spike generated by the circuit shown in plot (a).

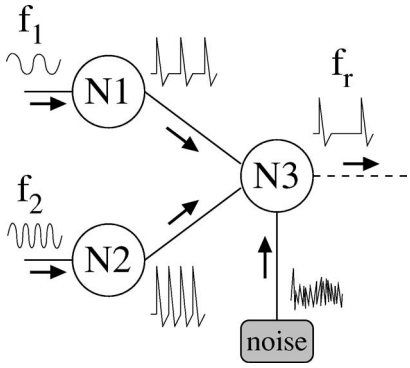

FIG. 2. Schematic representation of the experimental setup. Two excitable circuits are driven by two different frequencies f_1 and f_2, and their output is sent to a third processing circuit that will respond at a frequency f_r.

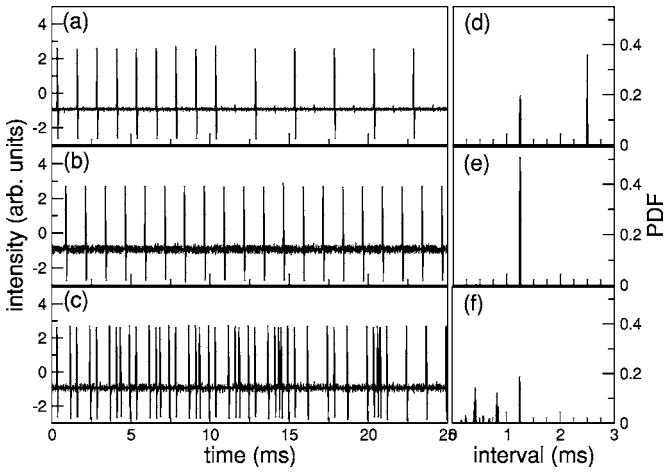

FIG. 3. Influence of the noise intensity in the spiking behavior of the system. The left-column plots show time series for increasing values of noise: (a) $V_{\mathrm{RMS}}=0.035$ V, (b) $V_{\mathrm{RMS}}=0.194$ V, and (c) $V_{\mathrm{RMS}}=0.270$ V. Plots (d)–(f) are the corresponding probability distribution functions of the interval between spikes. Intermediate values of noise intensity (b), (e) show an entrainment of the system at the ghost frequency $f_r=800$ Hz ($T_r=1/f_r=1.25$ ms).

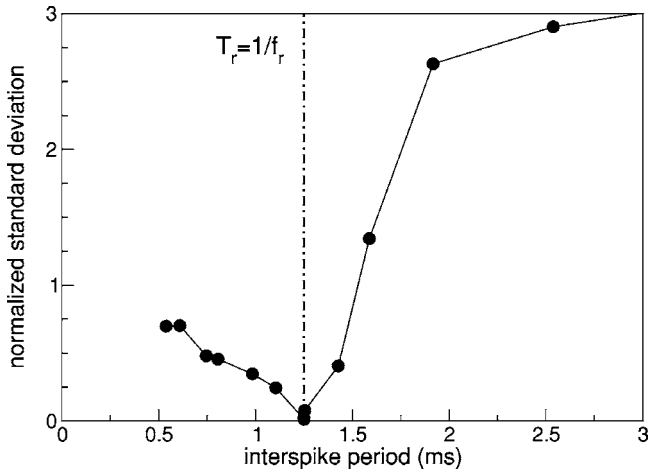

FIG. 4. Normalized standard deviation of the interspike interval vs its mean. The different measurements correspond to increasing values of noise. The minimum of the standard deviation corresponds to the entrainment of the system at the ghost period ($T_r=1/f_r=1.25$ ms).

first set $f_1=1600$ Hz and $f_2=2400$ Hz, which correspond to $k=2$, $f_0=800$ Hz, and $\Delta f=0$. The peak voltages that the processing circuit receives from the two input circuits are equal ($V_{1p}=V_{2p}=0.35$ V) and, as explained above, chosen so that their sum is still below the spiking threshold of that circuit ($V_{\mathrm{thr}}\sim 0.78$ V, determined by adjusting the gain of the voltage adder in the presence of only one spiking input). Due to that fact, an extra signal is needed in order to induce spikes at the output of the processing circuit. This signal is the noise, whose amplitude is controlled by the gain β of an electronic amplifier placed at the output of the noise generator. In order to have a quantitative value of the noisy signal amplitude, we calculate the root mean square voltage V_{RMS}.

The left-column plots of Fig. 3 show the time series of the output of the processing circuit for increasing values of the noise amplitude. The corresponding probability distribution functions (PDF) of the time interval between pulses are displayed in the right-column plots of the figure. Departing from a stable output, a small increase of the noise amplitude ($V_{\mathrm{RMS}}=0.035$ V) produces spikes at multiples of the ghost frequency [Figs. 3(a) and 3(d)]. For a further increase in the noise amplitude ($V_{\mathrm{RMS}}=0.194$ V) we can observe how the circuit responds exclusively at the ghost frequency, $f_r=800$ Hz [Figs. 3(b) and 3(e)]. The resonance holds during a certain range of noise amplitudes, and it is finally lost when noise becomes large enough ($V_{\mathrm{RMS}}=0.270$ V), as shown in Figs. 3(c) and 3(f). At this point, noise dominates the output and spikes occur at somewhat irregular periods; although the ghost frequency is still preferentially detected, the system responds also directly to the input frequencies. For even larger noise intensities (not shown), irregularity dominates completely the output of the processing circuit.

Figure 4 depicts a systematic study of the influence of noise in the frequency of the output pulses. The plot shows the normalized standard deviation of the interval between spikes vs its mean, corresponding to different values of the noise amplitude. The plot reveals clearly that the lowest standard deviation (i.e., the highest regularity) corresponds to a resonant period of $T_r=1.25$ ms, which matches the ghost resonance frequency $f_r=1/T_r=800$ Hz.

IV. INFLUENCE OF INHARMONICITY

Arrived at this point, it might seem that the ghost resonance is a simple response of the system to the difference between the input frequencies due to nonlinear mixing of oscillations ($f_r=f_2-f_1=2400-1600=800$ Hz). However, previous experimental realizations of GSR in the presence of inharmonic inputs indicate that this is not the case, since these inputs do not produce a response at the frequency difference [8]. We have performed here a similar set of experiments, in order to verify that the same conclusion applies in pulse-coupled architectures. To that end, we consider now a nonzero frequency detuning Δf at the input signals, following Eq. (1). This makes the signal frequencies incommensurate, while keeping their difference constant to $f_0=800$ Hz.

In the standard case in which the inputs are sinusoidal, an analysis of their linear superposition reveals a clear periodicity at the frequency [6]

$$f_r=f_0+\frac{\Delta f}{k+\frac{1}{2}}, \tag{2}$$

which is different from the frequency separation between the input signals (still equal to f_0), showing instead a linear dependence on the frequency shift Δf.

The same reasoning used in Ref. [6] to obtain Eq. (2), based on the analysis of the addition of sinusoidal signals, can be applied to all pairs of Fourier components of the input spike trains considered in our pulse-coupled case. Hence one can expect the processing circuit in our experiment to respond at a frequency obeying Eq. (2). This is indeed the case, as shown in Fig. 5. The figure compares experimental results

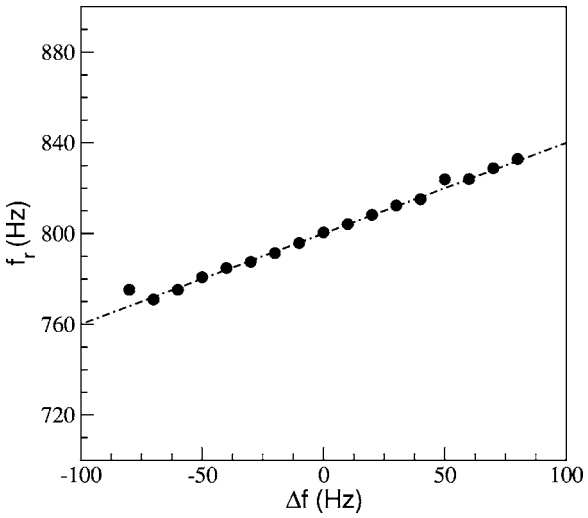

FIG. 5. Mean spike frequency of the processing circuit for varying frequency shift (Δf). The dashed line corresponds to the theoretical value of f_r given by Eq. (2) for $k=2$.

with the theoretical expression (2) for $k=2$, for the optimal noise level corresponding to $\Delta f=0$ [$V_{\mathrm{RMS}}=0.194$ V, the situation of Figs. 3(b) and 3(e)].

V. CHARACTERIZING THE RESPONSE TO INHARMONIC INPUTS

As was presented at length in previous work [6,7], the linear interference between harmonics leads to peaks that in the subthreshold case are easily detected by noise. It was also discussed that for relatively large noise intensity the system is triggered by other frequencies [see Figs. 1(c) and 1(d) of Ref. [7]]. In the present case, the input circuits respond in an all-or-none manner, transducing the (suprathreshold) input harmonic signals into spikes of constant amplitude. Thus the shape of the interference peaks is different from the sinusoidal case, there is no negative interference, and timing effects are more crucial. In this case the noise needs to be of the order of the pulse amplitudes in order to produce spikes at frequencies other than the ghost frequency, something that has no biological realism.

Here GSR requires the detection of the coincident arrival of spikes from the different harmonics into the processing element. Therefore the phases of the original harmonics being applied to the input circuits have to be carefully adjusted. In the particular case in which the input frequencies are multiples of a fundamental one [i.e., $\Delta f=0$ in Eq. (1)], the phase difference must be sufficiently close to zero so that the input spiking events coincide within a certain time interval. Numerical simulations of a neural model [13] have addressed this issue for spiking inputs, and shown that for realistic neural parameters the phase difference needs to be smaller than a few percent of the characteristic interspike interval, in order for coincidence detection to be effective (and thus for GSR to be present).

In the general inharmonic case [$\Delta f\neq 0$ in Eq. (1)] the role of the phase difference becomes pervasive, leading to the appearance of spike packages in the output of the processing element. Figure 6 shows an example of the output of the system when $\Delta f\neq 0$. This figure was obtained by fixing the noise amplitude at a value that ensures the observation of ghost resonance in the harmonic case $\Delta f=0$ ($V_{\mathrm{RMS}}=0.194$ V), and then increasing slightly the value of Δf. Under these conditions spikes appear in packages, so that the output is now characterized by three time scales: (i) the separation T_{spk} between spikes inside the packages, (ii) the interval T_{pkg} between consecutive spike packages, and (iii) the width ΔT of the spike packages. A similar behavior arises in the case of sinusoidal inputs, but in the present case the phenomenon is more robust, since it only operates during small time intervals (i.e., those in which spikes coincide), while most of the time the processing circuit is not responding.

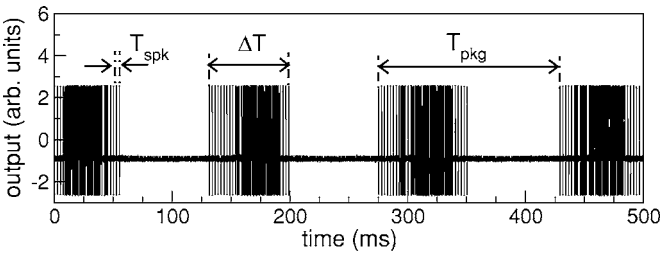

FIG. 6. Time series showing the influence of frequency detuning Δf in the output of the processing element.

The spike interval within packages is $T_{\mathrm{spk}}=T_r=1/f_r$, where f_r is the response frequency given by Eq. (2); in fact its inverse is the quantity plotted in Fig. 5. As explained above, this frequency arises from the superposition of the Fourier components of the two spike series. However, this argument only holds as long as spikes from the two series coincide in the processing circuit for a time long enough to excite the latter. This leads to the spike packages shown in Fig. 6, whose temporal characteristics are analyzed in the following.

A. Spike package frequency

Let us consider two spike trains of frequencies given by Eq. (1), and assume first that the spikes are δ shaped (i.e., they have zero width). Under this condition, two spikes coincide only when they occur exactly at the same time. In the case of $\Delta f=0$, this happens when

$$T_{\mathrm{coin}}=kT_1=(k+1)T_2, \tag{3}$$

where T_1 and T_2 are the input periods (inverse of the input frequencies f_1 and f_2). For $\Delta f\neq 0$ Eq. (3) is not valid anymore: the expected coincidence after a time kT_1 is lost because, given a perfect coincidence between two spikes (labeled a1 and b1 in Fig. 7), Δf produces a temporal shift between the next spikes that were supposed to coincide (a3 and b4 in Fig. 7). The value of this shift is given by

$$t_{\mathrm{shift}}=(k+1)T_2-kT_1=\frac{k+1}{(k+1)f_0+\Delta f}-\frac{k}{kf_0+\Delta f}. \tag{4}$$

Since $f_1<f_2$, the homogeneous shift Δf induces a higher relative increase in f_1 than in f_2, so that T_1 pulses move to

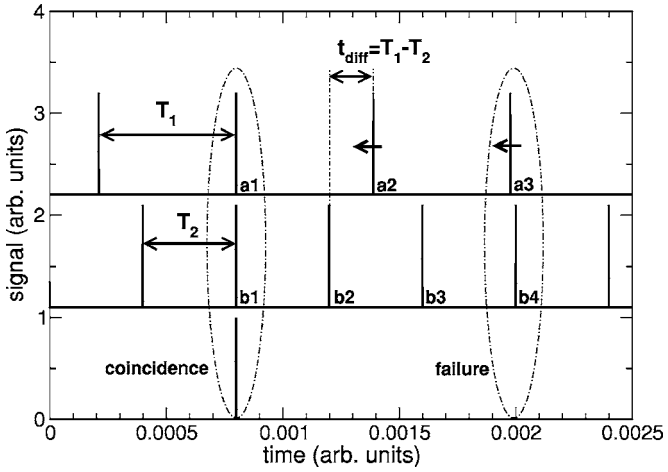

FIG. 7. Schematic representation of the coincidence-detection process for two inharmonic trains of δ-shaped spikes. The top panel represents the first input signal, the middle panel the second input signal, and the bottom panel the response of the processing element.

the left with respect to T_2. The next coincidence will then occur between the future images of spikes a2 and b2 in Fig. 7, which are the closest spikes. This will happen when the time difference $t_{\text{diff}}=T_1-T_2$ between a2 and b2 is filled by n consecutive shifts t_{shift}:

$$t_{\text{diff}} = nt_{\text{shift}}. \tag{5}$$

Using expression (4) and the fact that $t_{\text{diff}}=1/f_1-1/f_2$, with f_1 and f_2 given by Eq. (1), we find that the number n of "quasicoincidence" periods kT_1 needed to reach a new real coincidence is $n=t_{\text{diff}}/t_{\text{shift}}=f_0/\Delta f$. The interval between two perfect coincidences is the time from a1 to a2 (T_1) plus the time corresponding to these n quasicoincidence periods:

$$T_{\text{coin}} = T_1 + nkT_1 = T_1\left(1+\frac{f_0}{\Delta f}k\right) = \frac{1}{\Delta f}, \tag{6}$$

where the definition (1) has been used in the last equal sign. This result leads to a frequency between coincidences $f_{\text{coin}}=1/T_{\text{coin}}=\Delta f$.

The previous analysis has assumed δ-shaped input spikes. For spikes with finite width [see Fig. 1(b)] several coincidence events occur consecutively, giving rise to the spike packages shown in Fig. 6. The period of these packages, though, will still be given by Eq. (6). Figure 8(a) shows experimental results of the package frequency, f_{pkg}, compared with the theoretical prediction $f_{\text{pkg}}=f_{\text{coin}}=\Delta f$. The agreement shown is excellent.

B. Spike package width

As mentioned above, the nonzero width of the input spikes leads to several coincidence events in each spike package. Let us assume in what follows that the input spikes have the form of square-shaped pulses of width Δt_{spk}. We have already explained that Δf produces a temporal shift t_{shift} between quasicoincidence events (e.g., between pairs a1-b1 and a3-b4 in Fig. 7), whose value is given by Eq. (4). Due to

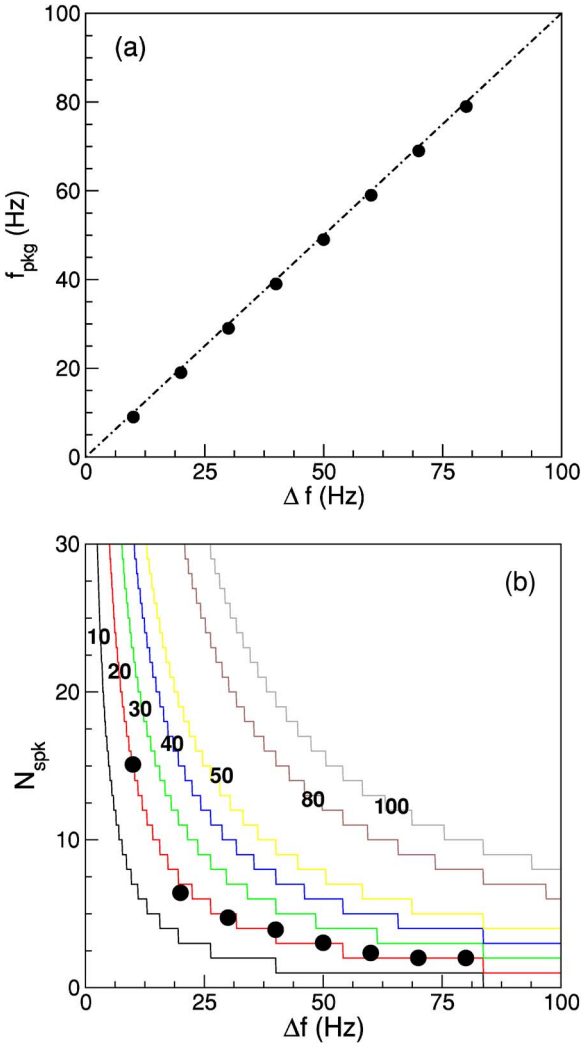

FIG. 8. (Color online) Package frequency f_{pkg} (a) and number of spikes per package N_{spk} (b) for increasing values of the frequency shift Δf. In (a), the dashed line corresponds to the theoretical value $f_{\text{pkg}}=\Delta f$. In (b), the lines correspond to the theoretical result (7) for different values of Δt_{spk} (in milliseconds). The staircase shape of those lines is due to the integer character of the spike number.

this shift, spikes a3 and b4 do not coincide if their width is zero. On the other hand, for spikes with nonzero width Δt_{spk}, coincidence holds until the accumulated shift is higher than Δt_{spk}. The total number of spikes within a package will be given by the number of times that t_{shift} is contained within Δt_{spk}:

$$N_{\text{spk}} = \frac{2\Delta t_{\text{spk}}}{t_{\text{shift}}} = \frac{2\Delta t_{\text{spk}}}{\Delta f}(kf_0+\Delta f)[(k+1)f_0+\Delta f], \tag{7}$$

where Eq. (4) has been used. The factor 2 that multiplies Δt_{spk} reflects the fact that spike-width-enabled coincidences occur both before and after a perfect superposition. This expression simplifies to $N_{\text{spk}}=2\Delta t_{\text{spk}}k(k+1)f_0^2/\Delta f$ for $\Delta f \ll f_0$. The temporal width of the spike package is $\Delta T=N_{\text{spk}}T_r$.

Figure 8(b) shows experimentally measured values of N_{spk} as a function of Δf, compared with the theoretical result (7) for different values of Δt_{spk} when square-shaped pulses are

considered. This comparison allows us to estimate the effective spike width to be $\Delta t_{\mathrm{spk}} \sim 20\ \mu$s.

VI. CONCLUSIONS

We have studied experimentally the integration and processing of distributed signals in pulse-coupled excitable electronic circuits via ghost stochastic resonance. Harmonic signals are applied to a set of detecting excitable circuits, which transduce the signals into spike trains that are further transmitted to a third processing circuit. For intermediate noise level this processing element exhibits a resonant response at a frequency not present in the input. We have studied the influence of inharmonic input frequencies by including a homogeneous frequency shift in all input components. This detuning leads to the appearance of pulse packages, which we have characterized in terms of their period and width. These observations should be taken into account when studying systems where information is transferred in a pulsed manner, such as in the nervous system.

ACKNOWLEDGMENTS

We thank Pablo Balenzuela for fruitful discussions. Financial support was provided by MCyT-FEDER (Spain, Project Nos. BFM2003-07850 and TEC2005-07799), and by the Generalitat de Catalunya.

[1] K. Wiesenfeld and F. Moss, Nature (London) **373**, 33 (1995).
[2] L. Gammaitoni, P. Hänggi, P. Jung, and F. Marchesoni, Rev. Mod. Phys. **70**, 223 (1998).
[3] V. S. Anishchenko, A. B. Neiman, F. Moss, and L. Schimansky-Geier, Usp. Fiz. Nauk **169**, 7 (1999) [Phys. Usp. **42**, 7 (1999)].
[4] A. Neiman and L. Schimansky-Geier, Phys. Rev. Lett. **72**, 2988 (1994).
[5] J. J. Collins, C. C. Chow, and T. T. Imhoff, Phys. Rev. E **52**, R3321 (1995).
[6] D. R. Chialvo, O. Calvo, D. L. Gonzalez, O. Piro, and G. V. Savino, Phys. Rev. E **65**, 050902(R) (2002).
[7] D. R. Chialvo, Chaos **13**, 1226 (2003).
[8] J. M. Buldú, D. R. Chialvo, C. R. Mirasso, M. C. Torrent, and J. García-Ojalvo, Europhys. Lett. **64**, 178 (2003).
[9] G. Van der Sande, G. Verschaffelt, J. Danckaert, and C. R. Mirasso, Phys. Rev. E **72**, 016113 (2005).
[10] O. Calvo and D. R. Chialvo, Int. J. Bifurcation Chaos Appl. Sci. Eng. (to be published).
[11] J. M. Buldú, C. M. Gonzalez, J. Trull, J. García-Ojalvo, and M. C. Torrent, Chaos **15**, 013103 (2005).
[12] C. Pantev, T. Elbert, B. Ross, C. Eulitz, and E. Terhardt, Hear. Res. **100**, 164 (1996).
[13] P. Balenzuela and J. García-Ojalvo, Chaos **15**, 023903 (2005).
[14] B. Grothe, Prog. Neurobiol. (Oxford) **61**, 581 (2000).
[15] R. Báscones, J. García-Ojalvo, and J. M. Sancho, Phys. Rev. E **65**, 061108 (2002).
[16] B. Lindner, J. García-Ojalvo, A. Neiman, and L. Schimansky-Geier, Phys. Rep. **392**, 321 (2004).